

Article

Production of Zirconium-Niobium Alloys for Nuclear Reactors Fuel Rods via SHS Process

Anatoly Mukhachev ¹, Dmytro Yelatontsev ^{1,2,*}  and Olena Kharytonova ²

¹ Institute of Geotechnical Mechanics Named by N. Poljakov, National Academy of Sciences of Ukraine, 2, Simferopolskaya St., 49005 Dnipro, Ukraine; map45@ukr.net

² Department of Metallurgy, Dnipro State Technical University, 2, Dneproetroevskaya St., 51918 Kamianske, Ukraine; eah@ukr.net

* Correspondence: sauron11652@gmail.com

Abstract: This article presents the results of studies of the self-propagating high-temperature synthesis (SHS) for obtaining zirconium alloys with niobium by the method of calcium-thermal reduction of nuclear-grade zirconium tetrafluoride in the presence of niobium powder. The optimal heating temperature of the initial charge and the methods of charge mixture with different calcium content were determined. The safety of the SHS process is ensured by the formation of an optimal combustion front of the mixture to remove the released high-pressure gases. A setup for the furnace reduction of zirconium alloys with charge preheating, discharge of molten products into molds of various designs, and control of the time and rate of slag and alloy crystallization has been tested. The required performance of the installation, the degree of transition of zirconium from salt into the alloy, and the purity, structure, and uniformity of the alloy were achieved.

Keywords: zirconium alloy; calcium-thermal reduction; self-propagating high-temperature synthesis; niobium



Citation: Mukhachev, A.; Yelatontsev, D.; Kharytonova, O. Production of Zirconium-Niobium Alloys for Nuclear Reactors Fuel Rods via SHS Process. *Alloys* **2023**, *2*, 157–167. <https://doi.org/10.3390/alloys2030012>

Academic Editor: Arne Mattias Thuvander

Received: 31 May 2023

Revised: 28 June 2023

Accepted: 7 July 2023

Published: 2 August 2023



Copyright: © 2023 by the authors. Licensee MDPI, Basel, Switzerland. This article is an open access article distributed under the terms and conditions of the Creative Commons Attribution (CC BY) license (<https://creativecommons.org/licenses/by/4.0/>).

1. Introduction

An alloy of zirconium with niobium is a unique structural material that has high corrosion resistance at elevated temperatures (up to 350 °C) and pressures, intense neutron, and gamma radiation [1]. The physical and mechanical properties of the alloy make it possible to use it as cladding for fuel rods containing uranium-235, which are used in the core of VVER-1000 and VVER-440 reactors [2]. In industry, this alloy is obtained by the fusion of pure metals, where the main component is a sponge or electrolytic zircon powder. Magnesium-thermal and electrolysis methods do not allow for obtaining zirconium alloys with a purity of more than 99.9% in a single-step process [3].

To obtain the Zircaloy-2 alloy, a zirconium sponge is alloyed with tin, nickel, chromium, and iron while using a 2–3-fold energy-consuming vacuum-arc remelting of pure metals. Similar technology is also used to obtain alloys E-110 and E-125 based on a mixture of powders, zirconium, and niobium in the Russian Federation [4].

Zirconium sponge and powder are obtained from insufficiently pure zirconium salts—zirconium chloride $ZrCl_4$ and potassium hexafluorozirconate K_2ZrF_6 , as a result of which the metal has a purity of 99.7–99.8%. The content of impurities (Fe, Cr, Ni, O_2 , N_2) in the zirconium sponge has a detrimental effect on the physicomaterial and radiation properties of the Zircaloy-2 alloy [5]. Therefore, the sponge is alloyed with these metals to obtain an ingot weighing up to 7 tons.

Electrolytic zirconium powder is a purer product than a sponge, but triple vacuum-arc melting was used to alloy it with niobium to obtain an ingot weighing up to 3 tons. These ingots are subjected to energy-intensive forging to obtain a cylinder with a diameter of 200 mm [6].

Vacuum-arc melting is not refining, but it allows for obtaining ingots of zirconium alloys of the required microstructure, with a uniform distribution of alloying elements [7]. Both methods make it possible to obtain tubular blanks weighing up to 50 kg in the course of multi-stage resource-intensive technological operations.

The development of electron-beam technologies has made it possible to intensify the process of purification of zirconium from metal impurities. This made it possible to obtain an alloy with a purity of more than 99.9% [8]. Electron-beam installations do not require the production of large-tonnage ingots, the melting of which requires an energy-intensive vacuum-arc process. They make it possible to obtain alloy E-110 from technical ingots after calcium-thermal reduction of zirconium tetrafluoride.

The processes of self-propagating high-temperature synthesis (SHS) of alloys became used on an industrial scale at the end of the 20th century [9]. A special place among their diversity is occupied by reduction-type processes using uranium and rare earth fluorides when sufficient heat is released during the reaction to melt the reaction products in the solid-solid system [10]. Zirconium and niobium are refractory metals, so their losses during electron beam melting are minimal. The use of calcium as a reducing agent made it possible for the first time to carry out the SHS process for obtaining metallic uranium and its alloys from tetrafluoride, in the form of an ingot weighing up to 10 tons [11]. This method is based on the low melting temperature of uranium and the high density of uranium (19 g/cm^3), which allows for the melting of reaction products and the complete separation of the metal and slag phases due to overheating.

The replacement of the magnesium-thermal and electrolytic methods for obtaining high-purity zirconium by the calcium-thermal process for obtaining alloys of reactor-grade zirconium with niobium in the SHS process is of scientific and practical interest.

Another example of the industrial application of the SHS process is the production of hafnium and REE for alloying refractory metals [12]. Recently, the production of an alloy of zirconium with silicon by the SHS method was studied [13]. Today, work is underway to improve and apply SHS processes in many countries of the world [14–17].

Alloys of refractory metals have found wide applications as structural materials for the production of products operating under conditions of high temperatures and pressures, radioactive fields, and cryogenic temperatures. At the same time, the methods of their production directly affect the physicochemical properties of alloys, which should provide not only the required product quality but also high process productivity.

With the development of high-tech industries, the demand for alloys based on refractory metals for the production of functional materials began to grow rapidly. This required the creation of less energy-intensive technologies for producing high-purity alloys at the level of ASTM standards (e.g., B350/B350M–11; B351/B351M–13; B352/B352M–17; B493/B493M–14; B495–10; B550/B550M–07; B551/B551M–12; B658/B658M–11).

Energy-saving technologies based on SHS reactions, which use internal energy to raise the process temperature above the melting point of the main component, are among the most economical [18]. To implement them, it is sufficient to use pure fluorides of refractory metals (zirconium, hafnium, uranium, and scandium) and available reducing agents (calcium, magnesium, aluminum). Mixing the components at room temperature provides uniformity at the stage of batch preparation. This ensures the production of alloys with low-temperature eutectics.

Metal-thermal reduction processes proceed at high speed and release heat, which allows for the quick melting of the metal and phase separation using different densities of slag. After separating a more fusible slag, the alloy is subjected to electron beam melting to remove volatile impurities and obtain a given ingot geometry, microstructure, and grain size [19].

This work aims to develop a safe scheme for the formation of a charge combustion front in a metal-thermal process with control of the reaction energy via the concentration, temperature, and kinetic factors, to ensure maximum process productivity and a high-quality zirconium-niobium alloy.

2. Materials and Methods

For the experiment, we used a sealed reactor made of stainless steel operating under a vacuum and in an inert argon atmosphere. A graphite crucible with a diameter of 500 mm and a height of 1800 mm was installed in the reactor, which was preliminarily heated in a vacuum at 1000 °C to remove moisture. The surface of the crucible was coated with calcium fluoride and niobium powder. The crucible was charged with a premixed mixture of zirconium tetrafluoride of different sizes, with different contents of the reducing agent (calcium shavings) in the presence of niobium powder.

The SHS reaction was initiated by an electric fuse placed with a mixture of zirconium tetrafluoride with calcium. It was located at the top of the charge. The retort was equipped with a safety valve to release the evolved gases.

The graphite crucible was prefabricated and consisted of a drawer and a metal receiver. In a graphite crucible, thermocouples were placed along the height, the combustion of which was used to determine the burning rate of the charge. The endpoint of the reaction was determined visually by the cessation of gas evolution. The process was carried out by out-of-furnace and furnace methods.

The reactor was evacuated after loading the mixture and filled with argon. After the reaction, the reactor was cooled in air and the reaction products were unloaded and weighed. Zirconium alloy ingots were separated from the slag and treated with nitric acid to dissolve surface impurities.

To determine the chemical composition of the ingot and its uniformity, samples were taken along the height and diameter of the ingot. An ingot with a diameter of 500 mm and a height of up to 100 mm was subjected to electron beam melting (EBM) to obtain an ingot with a diameter of 250 mm and a weight of up to 3.00 kg. The quality of the alloy was determined by comparing the chemical composition of the ingot; after the EBW, it was cut in height and diameter to study the physical and mechanical properties of the alloy.

For the experiment, zirconium tetrafluoride was used, obtained by the soda-extraction scheme, with a purity of 99.9%. It was purified from oxygen and nitrogen to 0.03% and 0.003%, respectively, by sublimation. The particle size of the salt was 1–6 mm. Calcium shavings with a specific surface of up to 40 m²/g were used as a reducing agent. The oxygen content in calcium was ≤0.1%, and nitrogen—≤0.005%.

To create an inert atmosphere, we used argon purified from impurities and traces of moisture up to 10⁻⁴%. Niobium powder with a particle size of 0.1–0.5 mm was used as the main alloying agent.

To carry out the process, a graphite crucible was used, in which the reduction zone was combined with the crystallization zone. The setups shown in Figures 1 and 2 were also used for the experiments.

An alloy of zirconium with a content of 1% niobium, obtained during the reduction melting, was tested for compliance with the following requirements (as per Ukrainian standard TU 001.257-85):

- Oxygen content in the range of 0.10–0.14 wt.%;
- Nitrogen content less than 0.005 wt.%;
- Carbon content less than 0.02 wt.%;
- The content of niobium 1 ± 0.1 wt.%;
- The content of hafnium is less than 0.005 wt.%;
- The content of CaF₂ in the ingot is less than 0.001 wt.%.

The ingot must be uniform in the content of alloying elements, niobium, oxygen, and impurities. The weight of the alloy ingot is determined by the safety of the process.

An alloy ingot with a diameter of 500 mm was subjected to electron-beam melting (EBM) on industrial units UE-182 and EMO-250, where the ratio of diameter to height varied from 5:1 to 1:3–1:4. In the alloy, hardness, impact strength, and ductility had been determined.

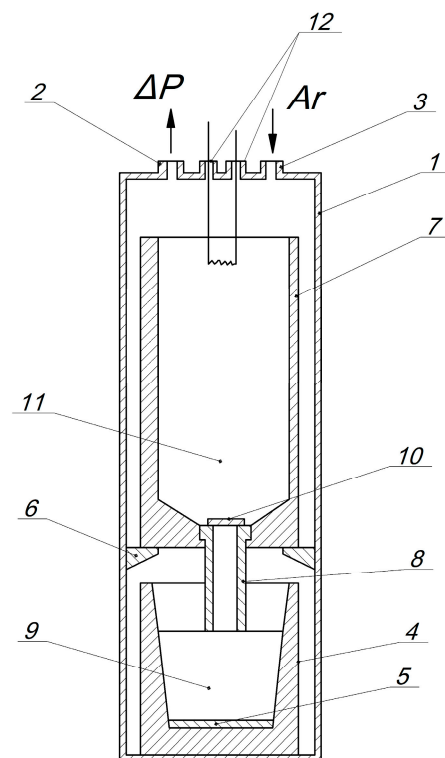


Figure 1. Scheme of the setup for obtaining a zirconium alloy with the discharge of reaction products into a chill mold: 1—sealed retort; 2—vacuum; 3—argon inlet; 4—chill mold; 5—backfill; 6—pawl; 7—graphite reactor; 8—drain channel; 9—ingot; 10—plug; 11—crucible; 12—fuse.

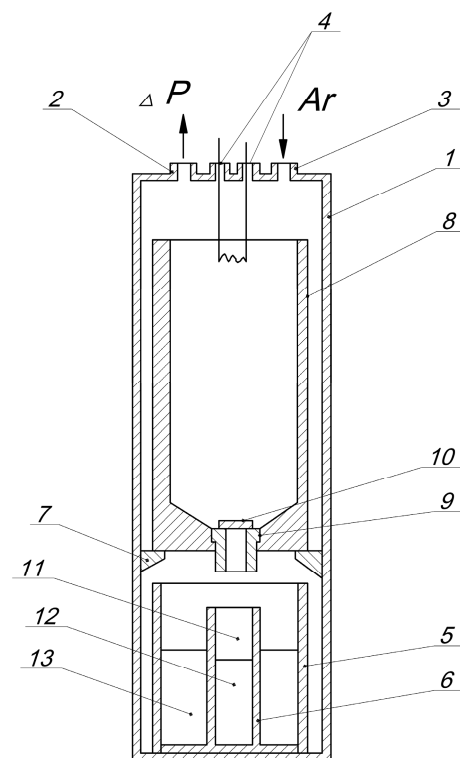


Figure 2. Scheme of the setup for zirconium alloy producing: 1—sealed reactor; 2—vacuum; 3—argon; 4—fuse; 5—crucible; 6—metal receiver; 7—pawl; 8—graphite reactor; 9—drain hole; 10—plug; 11—metal collector; 12—alloy ingot; 13—slag.

In a graphite reactor with a diameter of 500 mm and a height of 1800 mm, a cylindrical template with a given inner diameter was installed coaxially on the bottom. Inside the template, a pre-prepared mixture was loaded, consisting of calcium chips taken with a 15% excess, metal particles of the alloy-forming component, and zirconium tetrafluoride with a particle size of less than 2 mm. The space between the template and the reactor wall was filled to the same height with a charge consisting of calcium chips taken with a 5% excess, an alloy-forming component, and zirconium tetrafluoride with a particle size of 2–6 mm.

Then, the template was removed from the reactor and a layer of charge with a 5% excess of calcium, an alloy-forming component, and zirconium fluoride with a particle size of 2–6 mm was poured on top. The electrodes of the ignition device were immersed in the paraxial part of the charge surface. The reactor with the mixture was evacuated and filled with argon. By passing an electric current through the ignition device, a thermal reaction was initiated. After the reaction, the reactor was cooled, and the resulting ingot was separated from the slag and skull. The ingot was weighed and analyzed for the content of slag inclusions in it; the ledge was weighed.

The installation for carrying out the reduction reaction of zirconium tetrafluoride with calcium in the presence of an alloying agent, niobium powder, is shown in Figure 1.

To study the possibility of improving the quality of the alloy by reducing the content of carbon and impurities, a second installation was tested, the scheme of which is shown in Figure 2.

The device contains a sealed housing 1 with evacuation pipes 2, and an inert gas supply 3. A mold 4 is installed at the bottom of housing 1, which is protected from the inside by a layer of slag or reducing agent metal 5. In reactor 1, a pawl 7 is located coaxially above mold 4 on support 6, and tap hole 8 is installed coaxially. The height of graphite reactor 8 is equal to 0.8–1.2 of the height of the melt of product 11 in reactor 7 before it is drained. The inner diameter of drain hole 9 is equal to 1/14–1/18 of the inner diameter of reactor 7. The thickness of plate 10 is equal to 1/14–1/42 of the inner diameter of tap hole 8. The thickness of the standing slag or reducing agent metal 5 at the bottom of mold 4 is 1/90–1/150 of the height of the melt jet flowing from tap hole 8.

A graphite mold with an inner diameter of 600 mm and a height of 850 mm was installed in a sealed steel retort with an inner diameter of 800 mm and a height of 3100 mm. The bottom was protected by a layer of slag from reduction melting or by a calcium plate. A graphite reactor with an inner diameter of 600 mm and a height of 2000 mm was installed coaxially above it. At the bottom of the reactor, there was a hole into which a graphite tap-hole was inserted, the outlet of which was covered with calcium plates.

The reactor was loaded with zirconium fluorides weighing 120–170 kg per metal, broken calcium (in 5% excess), and niobium alloying metal. The system was evacuated and filled with argon, and the reaction was initiated using an electric igniter. The reaction products were poured into the crystallizer. After their cooling, the mold was removed from the retort and replaced with a new one for the next reduction melting. The products were weighed and the metal was analyzed for the content of impurities and slag inclusions. The mold was prepared for the next heat.

The influence of taphole dimensions, the thickness of calcium plates, and protective layers at the bottom of the mold on the results of reduction melts are shown in Table 1.

The content of gas impurities (hydrogen, nitrogen, oxygen), sulfur, and carbon in the alloy was determined using CS-230 LECO gas analyzers (USA). The content of metallic impurities was determined by the spectral method using a PGS-2 spectrograph, with the registration and spectra processing performed by the system for multi-element registration, MAES.

Table 1. Influence of melting conditions on alloy quality indicators.

Tap Hole Diameter (mm)	The Ratio of Taphole Diameter to Reactor Diameter	Loss of Metal in the Skull (wt.%)	Carbon Content in Metal (wt.%)	The Presence of Slag Inclusions in the Metal
50	1/12	1	>0.2	Yes
42	1/14	1–2	0.04–0.20	No
38	1/16	2.0–2.5	0.01–0.04	No
34	1/18	3–4	0.001–0.010	No
30	1/20	15	<0.001	No

3. Results

The study of the interaction between zirconium tetrafluoride and calcium made it possible to determine the parameters of charge preheating in vacuum and argon.

It has been established by differential thermal analysis that the spontaneous initiation of the reaction and its transition to the thermal explosion mode occurs at temperatures of 876–907 °C and 775 °C, respectively. It has been established that the reaction rate increases when the mixture is heated in a vacuum. Spontaneous heating of the charge already at 600 °C determines the onset of a thermal explosion. Reaching a temperature of 500 °C is a signal for the initiation of the SHS reaction.

The content of oxygen in the alloy depends on its content in ZrF_4 (≤ 0.03 wt.%) and in calcium (≤ 0.1 wt.%). The oxygen content in the alloy is 0.12–0.17%, which does not impair the ductility of the alloy because oxygen is an alloying element for zirconium.

In the course of melting in the out-of-furnace process with a common zone of reaction and crystallization, a yield of zirconium into an alloy ingot of 96% was achieved. However, the service life of the crucible was unstable as a result of the overflow sticking to the wall.

In a stationary crucible, the processing time is determined by the charge combustion rate, and the crystallization time is determined by the cooling conditions. The alloy remains in the molten state until the slag begins to crystallize. This period does not exceed 20–30 min, which allows lighter slag to float at a temperature of 1418 °C and stand out from the melt.

During the reaction, the temperature in the system rises to 1900–2200 °C, depending on the charge heating.

This method of carrying out the recovery process requires a long time to cool the reaction products and the crucible, which reduces the productivity of the installation.

The main disadvantage of the method of combined charging in a combined crucible is that the reaction front initiated in the center of the top of the charge propagates along the central axis of the load ahead of its peripheral layers. This leads to the fact that the reaction products ejected along the normal to the reaction front end up in the upper part of the reactor. The gas of the excess reducing metal and the desorbed gases rush upward and froth the molten reaction products. This leads to an increase in the contact surface of the alloy with the reactor, to an increase in the skull and sedimentation time in the metal phase. As a result, the degree of slagging of the resulting ingot increases.

The loss of metal in the skull averaged 4–7%, and the slag content in a compact draft ingot was at the level of 0.7–1.5 wt.% for reduction melts with a load of 120 kg of zirconium.

The effect of an excess of a reducing agent on the yield of metal into an ingot and its slagging was studied. The results are presented in Table 2.

Table 2. Influence of the particle size of the reduced compound and the excess of the reducing agent on the output of the metal into the ingot and its slag content.

No.	Charge Characteristics				Characteristics of the Metal		
	Inner Part		Outer Part		Content of CaF ₂ (wt.%)	Skull (wt.%)	Ingot Yield (wt.%)
	ZrF ₄ Particle Size (mm)	Exceeding Ca (wt.%)	ZrF ₄ Particle Size (mm)	Exceeding Ca (wt.%)			
1	1	5	2	1	0.007	5.6	94.4
2	1	10	2	3	0.008	4.0	96.0
3	2	10	2	1	0.005	3.0	97.0
4	2	15	4	3	0.004	2.1	97.9
5	2	20	6	5	0.005	1.5	98.5
6	3	20	7	5	0.056	3.5	96.5
7	3	25	8	8	0.070	4.2	95.8

The optimal conditions are an excess of calcium up to 10% with a ZrF₄ particle size of 2–6 mm.

The effect of particle size and excess reducing agent when dividing the filling zone into two parts is shown in Table 3.

Table 3. Influence of the ratio of the diameter and height of the backfill on the output of the metal into the ingot and its slag content.

No.	The Ratio of the Diameter to the Inside of the Backfill	The Ratio of the Total Height of the Backfill to the Height of Its Inner Part	Content of CaF ₂ in Metal (wt.%)	Loss in the Skull (wt.%)	Ingot Yield (wt.%)
1	1.0	0.90	0.003	5.8	94.2
2	1.0	1.01	0.003	4.2	95.8
3	1.2	1.01	0.004	2.6	97.4
4	1.5	1.10	0.004	1.8	98.2
5	1.8	1.20	0.005	2.2	97.8
6	2.0	1.20	0.007	2.2	97.8
7	3.0	1.50	0.012	1.9	98.1

4. Discussion

The optimal ratio of the diameters of the reactor and the inner backfill zone is 1.5. The content of slag in the ingot does not exceed 0.004 wt.%. The output of metal in the ingot reaches 98%.

In a separated charge, the reaction front, after its initiation in the axial part of the top, due to a smaller excess of calcium and a higher gas permeability of the shelled charge layer, first propagates mainly along the direction from the axial part of the top of the charge to its periphery and from top to bottom, and then, during combustion, already the bulk of the charge, in the direction of the normal to the cylindrical surface of the charge, from the periphery to the center. Here, during the combustion of the shelled layer of the charge, there is a smaller excess of calcium, therefore, there is less heat loss associated with heating, melting, and evaporation of excess calcium. In this zone, the charge porosity is increased. Consequently, there is also a deeper penetration of hot gases into it, which improves the conditions for the propagation of the reaction front in it. In this case, the remaining part of the charge has a reaction front in an area, almost equal to the full surface of its cylindrical volume. This leads to a decrease in the total time of combustion of the mixture and increases the release of the heat of the exothermic reaction. In addition, at the last stage of combustion of the charge, the reaction products, under the action of a force arising from the action of frontal gases on them, are thrown onto the reactor wall, block receiving surface, or the surface of the skull formed at the preliminary stage, and are separated from the gas, which freely exits through the annular gap that remained after the combustion of the shelled layer

of the charge. Products without foaming flow down to the bottom of the reactor. All this leads to significant overheating of the reaction products and the formation of conditions that provide a decrease in the volume of metal crystallized on the walls of the reactor in the form of a skull.

In order to eliminate these shortcomings, an installation was developed with the allocation of a crystallization zone by draining the reaction products into a mold. This made it possible to extend the service life of the crucible up to 10 cycles. Crystallization of the reaction products in the reduction reactor in an inert atmosphere led to the appearance of a skull weighing up to 7% of the weight of the ingot when the reactor was loaded with zirconium tetrafluoride in an amount of up to 170 kg. The reaction and crystallization zones are separated by a plug made of a 2 mm thick reducing metal plate to delay the melt drain and accumulate a certain volume of it, which melts calcium with a melting point of 660 °C. The melt begins to rotate and merge at a constant speed.

Due to the intensive rotation of the melt in the bottom part of the reactor, the formation of stagnant zones is excluded and the degree of crystallization of the metal in the reactor decreases. Draining the melt at a constant rate reduces its residence time in the reactor and, as a result, reduces the degree of crystallization of the metal in the reactor and its loss in the ledge. If there is no mixing of the melt during draining, and the drain rate gradually decreases, then the time spent by the metal in the stagnant zones in the bottom part of the reactor increases, and the degree of its crystallization in the reactor and drain hole increases.

The reaction products were poured from the reactors into the crystallizer at a constant rate of 150 L per minute. The constancy of the flow rate of the melt from the reactor was ensured by the indicated ratio of the sizes of the reactor and the drain hole. The flow rate of the melt flowing out of the reactor was recorded by the burnout of thermocouples located at the bottom of the mold and by the height of the melt filling the mold. The rotation of the melt flowing out of the reactor was observed through a viewing window. The results of recovery heats are presented in Table 4.

Table 4. Influence of the thickness of the calcium layer and ratio of the height of the calcium layer at the bottom of the mold on the ingot properties.

The Thickness of the Calcium Layer (mm)	The Ratio of the Height of the Calcium Layer at the Bottom of the Mold to the Height of the Flowing Melt Jet	The Content of Calcium in the Metal (wt.%)	Carbon Content in Metal (wt.%)	The Presence of Slag Impurities
5	1/90	>0.05	<0.001	Yes
3	1/150	0.02	0.001–0.010	No
2	1/225	0.01	0.01–0.04	No
1	1/450	0.01	0.05–0.10	No
0.5	1/900	<0.01	>0.1	No

A variant of the device was chosen, where a graphite reactor with an internal protective coating was installed under a stationary graphite reactor on one axis.

The taphole height is 0.8–1.2 of the melt height in the reactor. On the receiving surface of the mold, there is a plate of calcium with a thickness of 1/150–1/450 of the height flowing from the tap hole of the melt jet. The specified ratio of the height and diameter of the taphole provides self-regulation of the constancy of the melt outflow rate and eliminates the formation of stagnant zones in the reactor due to the centrifugal-siphon effect of auto-stabilization of the liquid outflow rate through a round hole in the bottom of the vessel, which is due to the centrifugal force of the melt rotation in the near-wall layers and the presence of funnel formation in it.

With an increase in the flow rate of the melt from the tap hole, the speed of rotation of the melt in the reactor increases, which leads to the pressing of the melt against the wall, and increases the size of the funnel at the drain hole.

Reduction melts of zirconium are intense in terms of heat balance since the released heat is quickly lost and is not enough to overheat the reaction products by more than 300–350 °C. This circumstance requires the reduction of heat losses to increase the time of the process of separation of the metal and slag phases. This idea was implemented in an experiment with the device shown in Figure 2. The purpose of the experiment was to reduce the volume of the shrinkage cavity in the alloy ingot and reduce the carbon content in the ingot to 0.01% and slag to 0.001%.

In metallurgy, there are methods for eliminating the shrinkage cavity by rapidly cooling the ingot by blocking heat removal from the side surface of the ingot using thermal insulation. However, this technique slightly reduces the size of the shrinkage cavity.

After the initiation of the reaction, the molten products were poured into the metal receiver, and part of the slag overflowed through its walls and blocked the outer surface of the mold. This led to the crystallization of the slag in the up-down direction, and the metal—bottom-up. Heat removal from the side surface was blocked by liquid slag.

The correct choice of the ratio of the height of the slag in the metal receiver at the level of 1/3–1, and in the slag receiver at the level of 1–2, the height of the metal receiver provides control over the processes of crystallization of slag and alloy

The presence of a slag layer in the metal receiver on top of the alloy with a height equal to the height of the metal leads to the formation of a vacuum cavity between the slag and the molten alloy. This creates the effect of vacuum-bottom metal cleaning.

The placement of the metal receiver inside the slag receiver ensures that the metal remains in a molten state for a longer time. This allows the slag to float almost completely and clean the metal. The thickness of the graphite wall was 1/10 of the inner diameter of the metal receiver. The ratio of the cross-sectional areas of the metal receiver and the slag receiver equal to 1/3–1/4 is optimal for the stability of the process of slag separation and metal crystallization. The thinner wall thickness of graphite does not withstand the impact of the molten jet of reaction products.

Analysis of the physicochemical and mechanical properties of the zirconium alloy with 1% niobium was carried out in the NSC KIPT (Kharkiv, Ukraine). The results of the studies are described in papers [20,21]. They confirmed the conformity of experimental alloy performance properties of the industrial analog, obtained from the electrolytic powder niobium by vacuum-arc melting.

Analysis of the chemical composition of the alloy showed full compliance with the specifications for the content of the main component and impurities. The distribution of the alloying components, niobium, and oxygen over the volume of the ingot, both after the reduction of zirconium fluoride and after EAF, was equally uniform.

5. Conclusions

- (1) For the first time, the method of safe production of zirconium alloy with 1% niobium by calcium-thermal reduction of zirconium tetrafluoride in the presence of niobium powder has been developed and experimentally tested.
- (2) Units for the reduction of zirconium tetrafluoride by calcium to produce zirconium alloy with 1% niobium with productivity up to 170 kg per melting have been developed and tested. The proposed method of SHS reaction provides the graphite crucible stability during 10 melts.
- (3) The safety of the SHS process is ensured by dividing the charge zones of the materials in the crucible into internal and external zones with different calcium excess. As a result, a stable charge combustion front without uncontrolled gas emissions is ensured.
- (4) Separation of the reduction and crystallization zones of the alloy by pouring the SHS reaction products into the crystallizer with the creation of the molten slag shell allows for a rarefaction in the upper part of the crucible, which leads to additional purification of the molten metal.

- (5) The conditions of effective separation of metallic and slag phases with the formation of a homogeneous alloy ingot with a minimum shell and uniform distribution of impurities and alloying components in the volume of the ingot have been studied and ensured.
- (6) The effect of vacuum-zone purification of the melt has been detected in the melts with the discharge of reaction products, which allows the reduction of the content of impurities at the expense of their transfer from the metal to the slag.
- (7) The combination of SHS processes of zirconium alloy with 1% niobium with ELP provides compact ingots with a diameter of 200 mm for the production of tube billets and tubes for fuel elements.
- (8) The properties of the experimental zirconium alloy with 1% niobium meet the requirements of international standard ASTM B350/B350M—11 (Reapproved 2016) and the standard of Ukraine TU 001.257-85.

Author Contributions: Conceptualization, A.M. and D.Y.; methodology, O.K.; software, O.K.; validation, D.Y. and O.K.; formal analysis, O.K.; investigation, D.Y.; resources, A.M.; data curation, A.M.; writing—original draft preparation, D.Y.; writing—review and editing, A.M.; visualization, D.Y.; supervision, A.M. All authors have read and agreed to the published version of the manuscript.

Funding: This research received no external funding.

Data Availability Statement: Data are unavailable due to privacy restrictions.

Acknowledgments: The authors thank the engineers Kuznetsov A.N. and Strel'tsov E.YA. for their technical support.

Conflicts of Interest: The authors declare no conflict of interest.

References

1. Lyubimova, L.L.; Tashlykov, A.A.; Buvakov, K.V. Roentgenometry of the Zr-2.5 Nb alloy under cyclic loads. *Int. J. Fatigue* **2019**, *126*, 381–389. [[CrossRef](#)]
2. Gurovich, B.A.; Frolov, A.S.; Kuleshova, E.A.; Maltsev, D.A.; Safonov, D.V.; Alekseeva, E.V. TEM-studies of the dislocation loops and niobium-based precipitates in E110 alloy after operation in VVER-type reactor conditions. *Mater. Charact.* **2019**, *150*, 22–30. [[CrossRef](#)]
3. Yuan, R.; Li, S.; Che, Y.; He, J.; Song, J.; Yang, B. A critical review on extraction and refining of vanadium metal. *Int. J. Refract. Metal. Hard Mater.* **2021**, *101*, 105696. [[CrossRef](#)]
4. Novikov, V.V.; Shishov, V.N.; Shevyakov, A.Y.; Voevodin, V.N.; Borodin, O.V.; Bryk, V.V.; Vasilenko, R.L. Investigation of the microstructure of zirconium alloys irradiated by zirconium ions in an accelerator. *At. Energy* **2014**, *115*, 307–312. [[CrossRef](#)]
5. Glazoff, M.V.; Tokuhira, A.; Rashkeev, S.N.; Sabharwall, P. Oxidation and hydrogen uptake in zirconium, Zircaloy-2 and Zircaloy-4: Computational thermodynamics and ab initio calculations. *J. Nucl. Mater.* **2014**, *444*, 65–75. [[CrossRef](#)]
6. Park, K.T.; Nersisyan, H.H.; Lee, H.H.; Hong, S.I.; Cho, N.C.; Lee, J.H. Low-temperature synthesis of zirconium metal using ZrCl₄-2Mg reactive mixtures. *Int. J. Refract. Metal. Hard Mater.* **2012**, *33*, 33–37. [[CrossRef](#)]
7. Cui, J.; Li, B.; Liu, Z.; Qi, F.; Zhang, B.; Zhang, J. Numerical investigation of segregation evolution during the vacuum arc remelting process of Ni-based superalloy ingots. *Metals* **2021**, *12*, 2046. [[CrossRef](#)]
8. Rodrigues, A.P.; Santos, P.M.; Veiga, J.P.; Casimiro, M.H.; Ferreira, L.M. Electron Beam Irradiation on the Production of a Si-and Zr-Based Hybrid Material: A Study by FTIR and WDXRF. *Materials* **2023**, *16*, 489. [[CrossRef](#)]
9. Merzhanov, A.G. History and recent developments in SHS. *Ceram. Int.* **1995**, *21*, 371–379. [[CrossRef](#)]
10. Mukhachev, A.P.; Kharytonova, O.A. Physicochemical fundamentals of a self-propagating high-temperature synthesis process of fabrication of alloys based on rare-earth metals. *Metallofiz. I Noveishie Tekhnologii* **2017**, *39*, 1395–1409. [[CrossRef](#)]
11. Vasudevamurthy, G.; Knight, T.W. Production of high-density uranium carbide compacts for use in composite nuclear fuels. *Nucl. Technol.* **2008**, *163*, 321–327. [[CrossRef](#)]
12. Parvizi, S.; Hashemi, S.M.; Asgarinia, F.; Nematollahi, M.; Elahinia, M. Effective parameters on the final properties of NiTi-based alloys manufactured by powder metallurgy methods: A review. *Prog. Mater. Sci.* **2021**, *117*, 100739. [[CrossRef](#)]
13. Zakaryan, M.K.; Kharatyan, S.L.; Aprahamian, A.; Manukyan, K.V. Combustion in the ZrF₄-Mg-Si and ZrF₄-Al-Si systems for preparation of zirconium silicides. *Combust. Flame* **2021**, *232*, 111514. [[CrossRef](#)]
14. Permin, D.; Postnikova, O.; Balabanov, S.; Belyaev, A.; Koshkin, V.; Timofeev, O.; Li, J. Influence of SHS Precursor Composition on the Properties of Yttria Powders and Optical Ceramics. *Materials* **2023**, *16*, 260. [[CrossRef](#)] [[PubMed](#)]

15. Kidalov, S.; Voznyakovskii, A.; Vozniakovskii, A.; Titova, S.; Auchynnika, Y. The Effect of Few-Layer Graphene on the Complex of Hardness, Strength, and Thermo Physical Properties of Polymer Composite Materials Produced by Digital Light Processing (DLP) 3D Printing. *Materials* **2023**, *16*, 1157. [[CrossRef](#)] [[PubMed](#)]
16. Vershinnikov, V.I.; Kovalev, D.Y. Formation of V₂AlC MAX phase by SHS involving magnesium reduction of V₂O₅. *Ceram. Int.* **2023**, *49*, 6063–6067. [[CrossRef](#)]
17. Xu, J.; Ma, P.; Zou, B.; Yang, X. Reaction Behavior and Formation Mechanism of ZrB₂ and ZrC from the Ni-Zr-B₄C System during Self-Propagating High-Temperature Synthesis. *Materials* **2023**, *16*, 354. [[CrossRef](#)]
18. Rosa, R.; Veronesi, P.; Leonelli, C. A review on combustion synthesis intensification by means of microwave energy. *Chem. Eng. Process. Process Intensif.* **2013**, *71*, 2–18. [[CrossRef](#)]
19. Mukhachev, A.P.; Pylypenko, M.M.; Kharytonova, O.A. Nuclear zirconium—the basis of alloys with improved neutron-physical, radiation, and corrosion properties. *Probl. At. Sci. Technol.* **2020**, *126*, 97–102. [[CrossRef](#)]
20. Mukhachev, A.P.; Kharytonova, O.A.; Evdokymova, T.A. Radiation tests of products made of calcium-thermal zirconium grade CTZ-110 under operation of the VVER-440 reactor. *Nucl. Phys. At. Energy* **2020**, *21*, 239–244. [[CrossRef](#)]
21. Vakhrusheva, V.S.; Voevodin, V.N.; Ladokhin, S.V.; Mukhachev, A.P.; Pilipenko, N.N. Production of nuclear reactors fuel tubes from Zr1Nb alloy cast billets of electron-beam melting. *Met. Cast. Ukr.* **2018**, *302–303*, 101–111. (In Russian)

Disclaimer/Publisher’s Note: The statements, opinions and data contained in all publications are solely those of the individual author(s) and contributor(s) and not of MDPI and/or the editor(s). MDPI and/or the editor(s) disclaim responsibility for any injury to people or property resulting from any ideas, methods, instructions or products referred to in the content.